The following publication Y. Yang, S. Ho, S. Tan and S. R. Hui, "Small-Signal Model and Stability of Electric Springs in Power Grids," in IEEE Transactions on Smart Grid, vol. 9, no. 2, pp. 857-865, March 2018 is available at https://doi.org/10.1109/TSG.2016.2569618.

Small-Signal Model and Stability of Electric Springs in Power Grids

Yun Yang, *Student Member, IEEE,* Siu-Shing Ho, Siew-Chong Tan, *Senior Member, IEEE,* and Shu-Yuen (Ron) Hui, *Fellow, IEEE*

***Abstract*—When multiple stable systems are combined into one system, the newly formed hybrid system has a certain possibility to be unstable. Such a natural phenomenon has been verified in the fields of chemistry and biology over the last century. The implementation of electric springs (ES) in large quantity over the power grids can also suffer from the same issue if specified design are not performed. As an initial feasibility study of multiple ES in smart grids, in this paper, based on the concept of relative stability, a method of tuning K_p and K_i of the proportional-integral (PI) controllers of the ES to ensure the overall system stability of a weak grid is investigated and is achieved through the aid of simulation on an extended low-voltage (LV) network of IEEE 13–node test feeder. Both simulation and experimental results validate that as the number of ES in the isolated LV network (weak grid) increases, more stringent values of K_p and K_i are required to achieve system stability. Besides, a hypothesis that if the optimal values of K_p and K_i are adopted, a maximum number of ES can be stably installed over the grid is proposed. It is also shown experimentally that by eliminating the instability of voltage fluctuation in the distribution line, the subsequent frequency fluctuation of the power generation can also be eliminated.**

***Index Terms*—Stability, electric spring (ES), small-signal model, low-voltage (LV) network, smart-load unit, smart grid, PI controller.**

I. Introduction

RENEWABLE energy sources like wind and solar energy will be increasingly used over the next few decades in many countries which are decarbonizing power generation [1]–[3]. These renewable energy sources will be massively and distributively installed in the power grids and as such, the traditional paradigm of centralized power flow control in that power generation follows the load demand on an instantaneous basis, will no longer be valid. This is because the unpredictable and intermittent nature of wind and solar makes it quite impossible for utility companies to precisely determine the instantaneous required power generation in real time. Instead, energy storage solutions [9], [10] and demand-side management strategies [4]–[10] in which load demand follows power generation upon activation have been proposed to alleviate the problem of real-time power fluctuation [6]–[8].

The idea of installing electric springs (ES) with non-critical loads as smart-loads was initially proposed in [11] for distributed voltage control while enabling demand-side management without the need for communication. ES can be used to i) provide electric voltage support; ii) store electric energy; iii) damp electric oscillations. ES that provide voltage control of grids through reactive power compensation are illustrated in [12]–[15]. A more comprehensive concept of ES, involving both active and reactive power compensation of power grids, was presented in [16]. So far, the reported investigations are mainly focused on the interaction of a single ES with the power grids [11]–[16]. In practice, multiple ES are required to be installed on different nodes along the distribution line of the low-voltage (LV) network to provide necessary voltage control of each local node. Apparently, with such an arrangement, the transmission of energy into the grid between various ES may cause instability of the combined grid system even if the individual ES system complies its respective stability design. It is well documented that multiple stable subsystems (no matter linear or nonlinear), with energy exchange between each other may cause the combined system to be unstable, as reported in [17], [18].

Such a phenomenon and some of its solutions are presented in the field of power electronics [19]–[30]. In [19]–[22], the small-signal analysis for the stability of power converters used for different areas are given. In [23]–[30], each grid-tied inverter is connected to the grid with a low impedance to achieve stability. However, the circumstance is changed if multiple inverters are connected to the grid in parallel. The stability of the system is then dependent on the total system's impedance. Parallel oscillation of the system between the inverters may occur. Furthermore, if the number of inverters is increased, the total capacitance of the system will be increased, which means that the resonant frequency will decrease. If the resonant frequency falls below the band frequency, the system will be unstable. In fact, all these analysis on the stability of multiple inverters in power system through circuit theories can essentially be explained using the more fundamental theory of local activity [18], which is a cornerstone theory for explaining the unstable phenomena in circuits. According to the theory of local activity, the unstable nature of multiple inverters with active loads is plainly attributed to the aspect of energy exchange between inverters and power sources. For multiple

Manuscript received October 13, 2015; revised February 22, 2016; accepted May 14, 2016. This work is supported by the Hong Kong Research Grant Council under Theme-based Research Project: T23-701/14-N.

Y. Yang, S. S. Ho, and S. C. Tan are with the Department of Electrical & Electronic Engineering, The University of Hong Kong, Hong Kong (e-mail: yangyun@eee.hku.hk, ssho@eee.hku.hk, sctan@eee.hku.hk).

S. Y. R. Hui is with the Department of Electrical & Electronic Engineering, The University of Hong Kong, Hong Kong and also with the Department of Electrical & Electronic Engineering, Imperial College London, London SW7 2AZ, U.K. (e-mail: ronhui@eee.hku.hk).

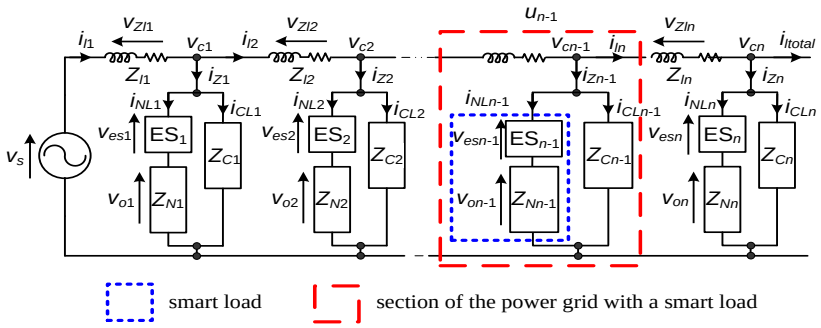

Fig. 1. Overview of electric springs embedded in smart loads that are installed along the distribution line of a power grid.

ES, such a phenomenon can also happen. The total resonant frequency of the system for multiple ES with *LC* filters is lower than the resonant frequency of system for a single ES, which can possibly fall below the band frequency of the system and leads to the instability of the system. Besides, as each ES is installed with batteries, the ES can be considered locally active. The energy transfer between power sources and each ES can introduce system instability, which severely affects the power quality of the electricity used by consumers and ruin the original purpose of ES in terms of stabilizing local node voltages supplying critical loads. More importantly, if the amplitude of the oscillation is significant and does not cease within the permitted period, the whole power system may blackout [31], [32]. Therefore, it is necessary to investigate the stability property of multiple ES when installed in the power grids and to provide the corresponding design solution. In this paper, the small-signal model and the stability analysis for multiple ES in both grid-connected LV network (strong grid) and isolated LV network (weak grid) are provided. The controllers used for the ES in this study are the classic PI controllers, which can achieve satisfactory performance in most applications involving both linear and nonlinear systems. Being compared with nonlinear control strategies, PI control generally requires less sensors. Besides, the structure of PI control is simple and the tuning method is mature, which is widely applied in industry. A tuning method of the PI controller of the ES in achieving stability for multiple ES implementation in the extended isolated LV network of IEEE 13–node test feeder is provided based on the analysis and simulation results. The proposed tuning strategy is also verified experimentally by three ES being installed in an emulated LV network. This method is generally applicable to the design of nonlinear types of controller for the same system.

II. Small-Signal Analysis of the Smart-load Unit

Fig. 1 shows an overview of a general power grid system with electric springs ES_j that are connected in series with the non-critical loads Z_{Nj} as smart loads. The smart loads are connected in parallel with the critical loads Z_{Cj}, where $j = 1, 2, \ldots, n$, and n is the total number of ES in this power network. Here, the node voltage of each ES is defined as v_{cj}. The current flowing through each smart load is defined as i_{NLj}, the current flowing through each critical load is defined as i_{CLj}, and the total current flowing through each unit of ES, smart load and critical load is defined as i_{Zj}. The voltage of each ES and non-critical load in smart load are respectively v_{esj} and v_{oj}. The ES and loads are powered by the voltage source v_s through the distribution cable which has sectional impedances described as Z_{lj}. The current flow of and voltage drop across the impedance are defined respectively as i_{lj} and v_{Zlj}. Each smart load, its parallel critical load, and the corresponding distribution cable impedance are defined as a smart-load unit.

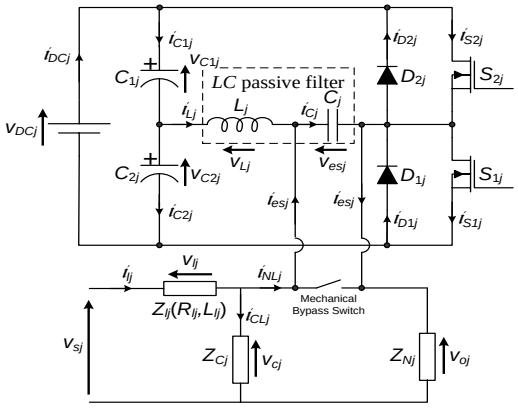

Fig. 2. Schematic of the smart-load unit.

The schematic diagram of the smart-load unit is given in Fig. 2. The ES is implemented by a half-bridge inverter. v_{sj} is the equivalent voltage source. By applying Kirchhoff's circuit laws and small-signal analysis [33], a general small-signal model for the smart-load unit can be obtained as

$$\begin{bmatrix} \dot{\widetilde{v_{cj}}} \\ \dot{\widetilde{v_{esj}}} \\ \dot{\widetilde{i_{Lj}}} \\ \dot{\widetilde{v_{sj}}} \end{bmatrix} = \begin{bmatrix} a_{1j} & a_{2j} & a_{3j} & a_{4j} \\ \frac{1}{C_j R_{Nj}} & -\frac{1}{C_j R_{Nj}} & \frac{1}{C_j} & 0 \\ 0 & -\frac{1}{L_j} & 0 & 0 \\ k_{1j} & k_{2j} & k_{3j} & k_j \end{bmatrix} \cdot \begin{bmatrix} \widetilde{v_{cj}} \\ \widetilde{v_{esj}} \\ \widetilde{i_{Lj}} \\ \widetilde{v_{sj}} \end{bmatrix} + \begin{bmatrix} 0 \\ 0 \\ \frac{V_{DCj}}{2L_j} \\ 0 \end{bmatrix} \widetilde{u_j}, \tag{1}$$

where $a_{1j} = \frac{R_{Cj}}{C_j R_{Nj}(R_{Cj}+R_{Nj})} - \frac{R_{Nj}R_{lj}+R_{Cj}R_{lj}+R_{Cj}R_{Nj}}{L_{lj}(R_{Cj}+R_{Nj})}$, $a_{2j} = \frac{R_{Cj}R_{lj}}{L_{lj}(R_{Cj}+R_{Nj})} - \frac{R_{Cj}}{C_j R_{Nj}(R_{Cj}+R_{Nj})}$, $a_{3j} = \frac{R_{Cj}}{C_j(R_{Cj}+R_{Nj})}$, and $a_{4j} = \frac{R_{Cj}R_{Nj}}{L_{lj}(R_{Cj}+R_{Nj})}$. Both critical and non-critical loads are pure resistive loads such that $Z_{Nj} = R_{Nj}$ and $Z_{Cj} =$

R_{Cj}, which will not affect the generality of the analysis. The impedance of the distribution cable Z_{lj} comprises the resistance R_{lj} and the inductance L_{lj}. The parameters k_{1j}, k_{2j}, k_{3j}, and k_j are time-varying coefficients adopted to model different kinds of power grids. A common classification of the grid is the so-called strong grid and weak grid. In a strong grid, the load current does not affect v_s. Therefore, the assurance of individual ES stability at a local node, when combined over the entire network, will result in a globally stable network. In a weak grid, load current disturbance affects v_s which affects node voltage. Individual ES stability does not ensure global stability of network. Investigation of the stability condition over the equivalent system model is required [34]. Based on the definition, $\sum_{i=1}^{3} k_{ij}^2 = 0$, $k_j \neq 0$ is adopted in the modeling of the strong grid and $\prod_{i=1}^{3} k_{ij} k_j \neq 0$ for the weak grid. Without considering additional state variables, the proposed models of both strong and weak grids can extensively (although not fully) reflect the dynamics of the system, e.g. impedance and load change.

III. Stability Analysis of the Smart-Load Unit

A. Derivation of the Transfer Function of the Controlled Smart-Load Unit

Based on (1), the frequency domain transfer function for each smart-load unit in Laplace form can be derived as

$$G_{cu}(s) = \frac{\widetilde{v_{cj}}(s)}{\widetilde{u_j}(s)} = \frac{G_{\omega 1j}(s) - G_{\omega 2j}(s)\frac{R_{Nj}V_{DCj}}{2L_j s}}{G_{\omega 2j}(s)}, \quad (2)$$

where $G_{\omega 1j}(s) = \frac{R_{Nj}V_{DCj}(s-a_{1j})(s-k_j)}{2L_jC_j(s-k_j)} + \frac{V_{DCj}a_{3j}(s-k_j)}{2L_jC_j(s-k_j)} + \frac{a_{4j}(k_{3j}V_{DCj}-k_{1j}R_{Nj}V_{DCj})}{2L_jC_j(s-k_j)}$ and $G_{\omega 2j}(s) = (s-a_{1j}) + \frac{-a_{2j}+\frac{a_{3j}}{L_j s}-\frac{a_{4j}\left(k_{1j}R_{Nj}C_j s+k_{1j}+k_{2j}+\frac{k_{1j}R_{Nj}-k_{3j}}{L_j s}\right)}{s-k_j}}{R_{Nj}C_j s+1+\frac{R_{Nj}}{L_j s}}$.

The controllers used for each ES in this paper are classic PI controllers with a transfer function $G_c(s) = K_p + \frac{K_i}{s}$, where K_p is the proportional gain and K_i is the integral gain. The transfer function of the controlled system is

$$\frac{\widetilde{v_{cj}}(s)}{\widetilde{v_{crefj}}(s)} = \frac{G_c(s)G_{cu}(s)}{1+G_c(s)G_{cu}(s)}, \quad (3)$$

where $\widetilde{v_{crefj}}(s)$ is the small-signal variation of $v_{crefj}(s)$, which is the reference voltage of v_{cj}. The transfer function (3) can also be used for the after-mentioned simulation to determine the effect of the coefficients on the power grid's behavior.

B. Brief Description on the Concept of Relative Stability

A useful method for determining the stability of a system in the frequency domain is by locating the eigenvalues in the s plane. If all eigenvalues are located on the left-hand side of the $j\omega$ axis, the system is stable. Otherwise, the system is unstable. The concept of relative stability states that the further the eigenvalues are located on the left, the more stable the system will be. Conversely, the further the eigenvalues are located on the right, the more unstable the system will be [35]. The transition from being stable to unstable is determined by the $j\omega$ axis, which is also known as the boundary of the stability. The relative stability concept can be understood from Fig. 3. Fig. 3(b) depicts the RMS value of the common coupling voltage v_{cj} of the system after a sudden change of v_s under a control corresponding to the eigenvalues presented in Fig. 3(a).

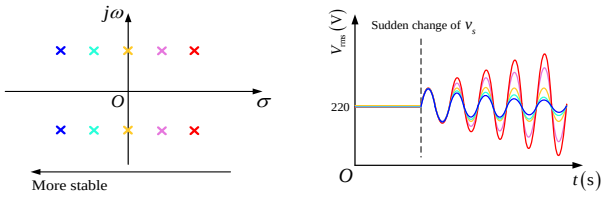

(a) Eigenvalues in s-plane (b) Corresponding waves

Fig. 3. Illustration of relative stability.

C. PI Controller Tuning Based on Eigenvalues

From (1) and (3), the Jacobian matrix of the controlled system can be obtained as

$$J(X_e) = \begin{bmatrix} a_{1j} & a_{2j} & a_{3j} & a_{4j} \\ \frac{1}{C_j R_{Nj}} & -\frac{1}{C_j R_{Nj}} & \frac{1}{C_j} & 0 \\ \frac{V_{DCj}}{2L_j}G_c & -\frac{1}{L_j} & 0 & 0 \\ k_{1j} & k_{2j} & k_{3j} & k_j \end{bmatrix}, \quad (4)$$

where $G_c = \frac{L^{-1}\left[(\widetilde{v_{crefj}}(s)-\widetilde{v_{cj}}(s))\left(K_p+\frac{K_i}{s}\right)\right]}{\widetilde{v_{cj}}}$ and $L^{-1}[.]$ is the inverse Laplace transform operator. From (4), the eigenvalues of the system can be found by solving

$$\det[\lambda I - J(X_e)] = 0, \quad (5)$$

for the eigenvalues λ, where I is a 4×4 matrix.

All eigenvalues should contain negative real parts to ensure full system stability. Reversely, for controller design, one can set the eigenvalue pairs on the $j\omega$ axis of the s plane, which represent the boundary of stability, i.e., $s = \pm mj$, where $m \geq 0$. Then, based on (4) and (5), the feasible ranges of K_p and K_i that can be used with stability assurance can be obtained. However, for multiple ES system, the rank of the Jacobian matrix can be five (or higher). According to Galois Theory, there is no formula for the roots of a fifth (or higher) degree polynomial equation in terms of the coefficients of the polynomial, using only the usual algebraic operations (addition, subtraction, multiplication, division) and application of radicals (square roots, cube roots, etc.) [36]. This implies that for a system with three or more ES, it is not possible to derive the stability criteria analytically. Nevertheless, it is feasible to numerically study the tuning parameters K_p and K_i via the simulation results, which will be presented in Section IV.

D. Effect of Local Voltage Instability on Global System's Frequency

In this paper, the power generator is modelled as an ideal source without considering the generator dynamics for simplicity of elaborating the possibility of frequency variation

when multiple ES are not well-regulated. A simple power generator of a power grid is governed by the swing equation [37]

$$J\omega_r \frac{d\omega_r}{dt} = P_m - P_e, \tag{6}$$

where J is the rotational inertia of the rotor, ω_r is the angular frequency of the generator, P_m is the mechanical turbine power, and P_e is the electrical power. The amplitude fluctuation of v_{cj} due to any instability will lead to the fluctuation of P_e, and may consequently (depending on the penetration level of the disturbance) fluctuates the frequency of the power generation, i.e., frequency of the system. Severe frequency fluctuation affects not only the power quality of the delivered electricity, but may induce more instability with some other load consumptions to further destabilize the entire network.

IV. Case Studies and Simulation Results

The control block diagram of the smart-load unit is shown in Fig. 4, where V_{crefj} is the RMS value of v_{crefj}, V_{cj} is the RMS value of v_{cj}, θ is the difference of angle between V_{oj} and i_{NLj}. The PLL adopted in Fig. 4 is the conventional PLL with a phase detection unit, a loop filter and a voltage controlled oscillator with a bandwidth of 25 Hz. The PLL in the final control strategy for the actual switched system is not included in the small-signal model, but it does not affect the values of tuning coefficients derived based on the small-signal analysis.

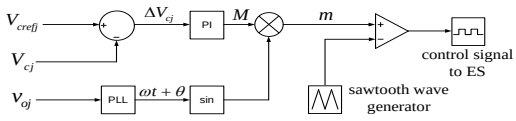

Fig. 4. Control block diagram of the smart load.

The parameters of each smart-load unit and the power source used in the simulation are given in Table I.

TABLE I
SPECIFICATIONS OF THE SMART-LOAD UNIT AND POWER SOURCE

Parameters	Values	Parameters	Values
$V_{\mathrm{DC}j}$	400 V	C_{1j},C_{2j}	3000 μF
L_j	500 μH	C_j	13.2 μF
$Z_{\mathrm{C}j}$	53 Ω	$Z_{\mathrm{N}j}$	50.5 Ω
L_{lj}	1.22 mH	R_{lj}	0.1 Ω
v_{sj}	350 sin $(\omega t+\theta)$ V	$v_{\mathrm{cref}j}$	311 sin (ωt) V
f_{ref}	50 Hz	f_{s}	20 kHz

A. ES in a Strong Grid

In this part, as shown in Fig. 5, simulation is performed on the IEEE 13–node test feeder with grid-connected mode of extended LV network (the breaker is on) with fluctuations of the renewable energy source v_s value systematically changing from 0% to 10% to -10% to 30% to -20% to 30% and finally to 20% of the nominal voltage (i.e., 220 V_{rms}) at every 1 s interval, for the case of with and without an ES. The installed

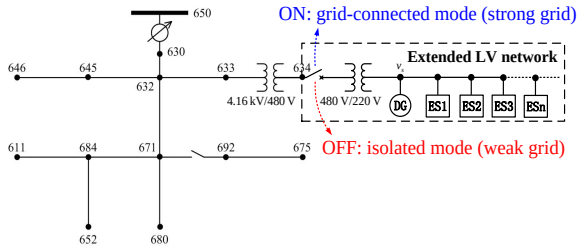

Fig. 5. IEEE 13–node test feeder with extended LV network in grid-connected and isolated mode.

ES adopts a PI controller with $K_p = 0.06$ V/V and $K_i = 0.0004$ V/V. The network has two voltage levels 4.16 kV and 480 V with a distribution transformer connected between node 633 and 644. In the original feeder, an aggregated load is connected to bus 634. However, for the purpose of this paper, the LV side has been modified to a 220 V distribution line with a step-down transformer of 480V/220V. Fig. 6 shows the corresponding RMS value of the critical load voltage. As shown, with the ES activated, the voltage of the critical load is regulated at the nominal RMS voltage of 220 V despite the fluctuations of v_s. However, without the ES, the voltage of the critical load fluctuates according to the fluctuation of v_s.

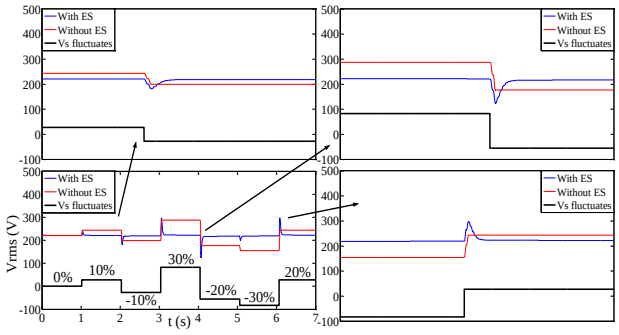

Fig. 6. Comparisons of the RMS voltage of the critical load for the case of with and without an ES, with v_s fluctuating.

Based on the parameters in Table I and by solving (5), the critical values of the PI controller, which correspond the boundary of stability, can be obtained as $K_p = 1.1$ V/V and $K_i = 9.2$ V/V. Therefore, the stable ranges of K_p and K_i of the PI controller for single ES in a strong grid can be given as

$$\begin{cases} 0 \text{ V/V} \leq K_p \leq 1.1 \text{ V/V} \\ 0 \text{ V/V} < K_i \leq 9.2 \text{ V/V} \end{cases}. \tag{7}$$

The critical values of K_p and K_i are dependent on the parameters in (4). To validate the calculated critical tuning values and further investigate the stability effect of multiple ES under these values, several sets of K_p and K_i values are used in the simulation of the critical load voltage. The results are shown in Fig. 7. Furthermore, in strong grids, the assurance of stability of a single ES is sufficient for assuring the stability of multiple ES in the same grid. As long as the droop control strategy is adopted [14], the tuning range of K_p and K_i in (7)

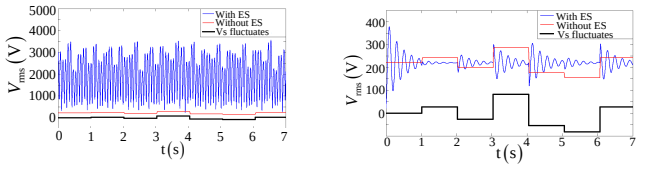

(a) $K_p = 0.06$ V/V, $K_i = 10$ V/V (b) $K_p = 0.06$ V/V, $K_i = 5$ V/V

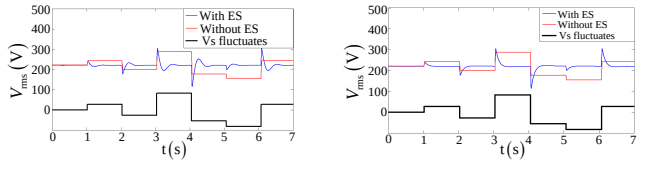

(c) $K_p = 0.06$ V/V, $K_i = 1$ V/V (d) $K_p = 0.06$V/V, $K_i = 0.25$V/V

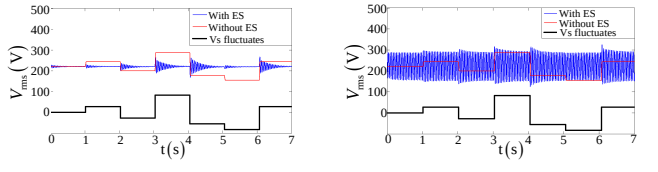

(e) $K_p = 1$ V/V, $K_i = 0.25$ V/V (f) $K_p = 1.5$ V/V, $K_i = 0.25$ V/V

Fig. 7. RMS voltage waveforms of the critical load under different K_p and K_i values for a single ES in a strong grid.

is also applicable for multiple ES in a strong grid.

B. ES in a Weak Grid

In (1), it is mentioned that different values of k_1, k_2, k_3, and k represent different impact levels of v_c, v_{es}, i_L and v_s on the variation of v_s, which mathematically describe how strong or weak the grid is. Based on (3), the pole-zero map of the controlled smart-load unit can be plotted as shown in Fig. 8. Considering (7) and the performance in Fig. 7, a conservative setting of $K_p = 0.2$ V/V and $K_i = 0.25$ V/V is used. According to Fig. 8(a), when $k_2 = 0$, $k_3 = 0$, $k = 0$, and the value of k_1 changes from 100 to 1000, one eigenvalue moves from the original point to the right-half plane, which means that as the influence of v_c on v_s increases, the smart-load unit tends to become more unstable. Similar conclusions on the increasing influence of v_{es} (as k_2 increases) and i_L (as k_3 increases) on v_s, which result in the smart-load unit becoming more unstable, can be drawn from Fig. 8(b) and 8(c), respectively. However, note that it is only for very large values of k_1, k_2, and k_3 that the stability issue of the weak grid system needs to be considered. In reality, K_p and K_i are more strictly tuned, which results in necessarily larger k_1, k_2, and k_3 values than that given in Fig. 8 for causing instability. This means that the the smart-load units can undertake a weaker grid than the one simulated for Fig. 8. Therefore, the ranges of K_p and K_i of the PI controller of a single ES in a weak grid can be the same as that for a strong grid.

Thus, $K_p = 1.1$ V/V and $K_i = 9.2$ V/V are the critical tuning of the PI controller corresponding to the boundary of stability for a single ES in a weak grid, which is implemented by an extended LV network in isolated mode of the IEEE 13-node test feeder, as shown in Fig. 5. Fig. 9(a) shows the RMS

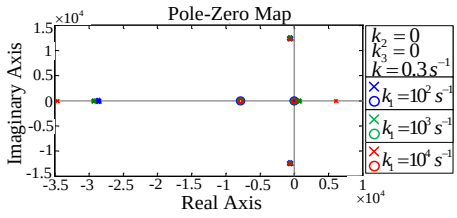

(a) Only k_1 value changes

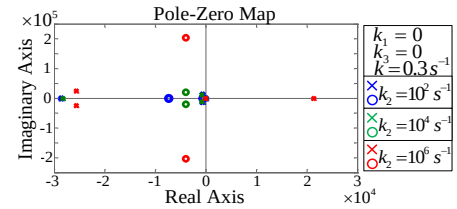

(b) Only k_2 value changes

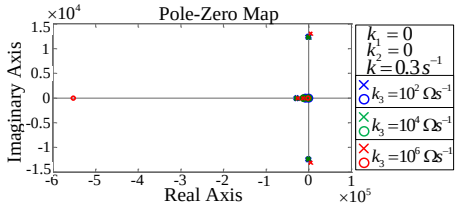

(c) Only k_3 value changes

Fig. 8. Poles and zeros of the smart-load systems in a weak grid with different values of k_1, k_2, and k_3.

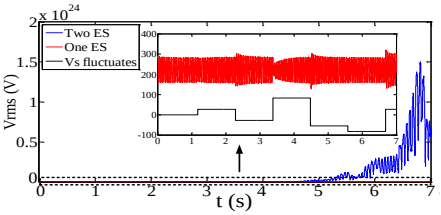

(a) $K_p = 1.1$ V/V, $K_i = 9.2$ V/V (critical tuning for one ES)

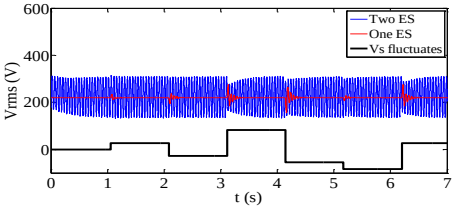

(b) $K_p = 0.7$ V/V, $K_i = 8.0$ V/V (critical tuning for two ES)

Fig. 9. RMS voltage waveforms of the critical load in the weak grid with one installed ES and two installed ES.

voltage waveform of the critical load of the system with a single ES and that with two ES installed in the weak grid, both with the critical tuning of $K_p = 1.1$ V/V and $K_i = 9.2$ V/V. With one ES, the system is at the boundary of stability with sustained oscillation. With two ES, the system is highly unstable. On the other hand, by substituting the specifications

in Table I into (7), critical values of $K_p = 0.7$ V/V and $K_i = 8.0$ V/V for two ES can also be obtained. Fig. 9(b) shows the corresponding RMS voltage waveform of the critical load. Obviously, with this setting, system with two ES are at the boundary of stability and that of single ES, via the concept of relative stability, is more stable than that of single ES with $K_p = 1.1$ V/V and $K_i = 9.2$ V/V. From this, it can be observed that as the number of ES in the weak grid increases, more stringent values of K_p and K_i are required.

As mentioned, there is no mathematical resolution for deriving the stability criteria of a grid with three or more ES. Nevertheless, the control design can be practically achieved through a parameter-tuning process via time-domain simulation. Here, we adopt a conservative approach such that as the values of K_p and K_i are changed, the dynamic response of the critical load's RMS voltage with one ES installed on the grid, are visually inspected. The parameters which generate one overshoot or undershoot in the critical load's RMS voltage without further oscillation when v_s fluctuates, are defined as the critical parameters of the PI controller. After several rounds of tuning, the critical parameters $K_p = 0.2$ V/V and $K_i = 0.25$ V/V are found to be the upper bound values for a single ES. The lower bound values for single ES are found to be $K_p = 0.05$ V/V and $K_i = 0$ V/V.

Through several repeated tuning of the PI controllers for the number of ES increasing from 1 to 10 and 50 and keeping K_i at 0 V/V $< \mathrm{K_i} \leq 0.25$ V/V, the tuning ranges of K_p can be obtained. Then, by tuning K_i and adjusting K_p within a small range, the final tuning range of K_p and K_i of the PI controllers can be determined as given in Table II. Visual plots of the tuning for different number of ES that achieve system stability are given in Fig. 10. Fig. 10(b) is the two-dimensional view from top of Fig. 10(a).

TABLE II
TUNING RANGE OF K_P AND K_I FOR DIFFERENT NUMBER OF ES IN THE WEAK GRID

Number of ES	Range of K_p (V/V)	Range of K_i (V/V)
1	$0.05 \leq K_p \leq 0.2$	$0 < K_i \leq 0.25$
2	$0.05 \leq K_p \leq 0.14$	$0.01 < K_i \leq 0.1$
3	$0.05 \leq K_p \leq 0.12$	$0.03 < K_i \leq 0.1$
4	$0.05 \leq K_p \leq 0.09$	$0.04 < K_i \leq 0.1$
5	$0.05 \leq K_p \leq 0.09$	$0.04 < K_i \leq 0.1$
6	$0.05 \leq K_p \leq 0.09$	$0.04 < K_i \leq 0.1$
7	$0.05 \leq K_p \leq 0.09$	$0.05 < K_i \leq 0.1$
8	$0.05 \leq K_p \leq 0.08$	$0.05 < K_i \leq 0.1$
9	$0.05 \leq K_p \leq 0.07$	$0.05 < K_i \leq 0.1$
10	$0.05 \leq K_p \leq 0.07$	$0.05 < K_i \leq 0.1$
50	$0.05 \leq K_p \leq 0.065$	$0.06 < K_i \leq 0.1$

From Fig. 10(b), the optimal parameters of $K_p = 0.05$ V/V and $K_i = 0.1$ V/V can be found. This means that if all the controllers of ES are tuned with $K_p = 0.05$ V/V and $K_i = 0.1$ V/V in the weak grid, the maximum number of ES can be installed. Besides, if the weak grid system requires only stability and are not concerned with the dynamics, the tuning range of K_p and K_i can be larger than the tuning values obtained with the defined conservative approach. Furthermore, based on the tendency of tuning results in Fig. 11, which shows that keeping the critical tuning of K_p and K_i for 50

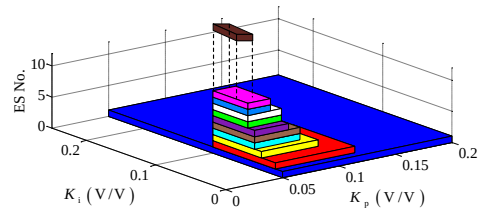

(a) Three-dimensional view

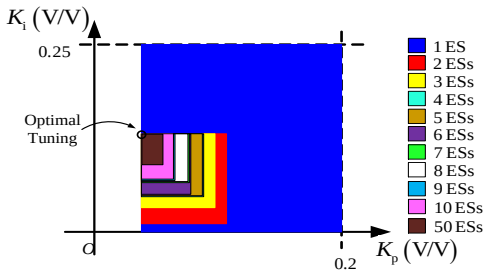

(b) Two-dimensional view

Fig. 10. Tuning zones of K_p and K_i for different number of ES in the weak grid.

ES, the system can be more stable when the total number of ES is reduced, and also the results in Fig. 9(b), the values of K_p and K_i can be fixed and need not be adjusted according to the number of ES being installed, since the system with the optimal tuning of K_p and K_i can tolerate light variations of the system conditions. Even if the variation of the system conditions is heavy, by using the results given in Fig. 10, a trail-and-error method of increasing/decreasing both the values of K_p and K_i of the system to achieve system stability, can be conducted.

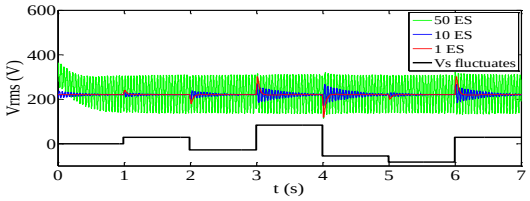

Fig. 11. A comparison of the RMS voltage waveform of the critical load in a weak grid containing 50 operating ES, 10 operating ES, and 1 operating ES, all with the critical tuning for 50 ES.

TABLE III
SPECIFICATIONS OF THE SECTION OF THE POWER GRID WITH A SMART LOAD FOR EXPERIMENT

Parameters	Values	Parameters	Values
V_{cref}(rms)	30 V	V_s(rms)	31.32 V
C_1	1640 μF	C_2	1640 μF
L	500 μH	C	13.2 μF
L_l	0.5 mH	J	3.5 kg$\times$m^2
V_{DC}	48 V	f_s	20 kHz

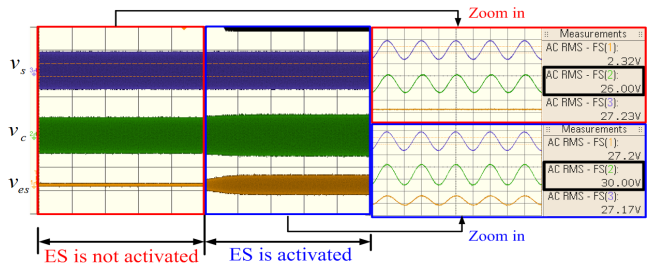

Fig. 12. Waveforms of the renewable energy voltage v_s, common coupling point voltage v_c, and voltage of ES for single unit of smart load.

V. Experimental Verification

Experiments are conducted on three units of smart load with the main parameters given in Table III. The non-critical load used for each unit is a nominal 60 W bulb and a nominal 200 W bulb in parallel. The critical load used for each unit is a 50 Ω resistor. The PI controllers are implemented using TI's TMS320F28069. The variable energy source is emulated by the California Power Supply CSW5550 with MATLAB/SIMULINK.

The effectiveness of using ES to regulate the voltage of the common coupling point can be seen in Fig. 12. As the RMS voltage of the variable energy source v_s is reduced from 31.32 V to 27.21 V, the RMS voltage of the common coupling point v_c is decreased from 30 V to 26 V before the ES is activated. However, after the ES with PI controller of $K_p = 0.05$ V/V and $K_i = 0.008$ V/V is activated, v_c rises back to the nominal 30 V.

Then, two units of smart load with the same PI controller tuning of $K_p = 0.05$ V/V and $K_i = 0.008$ V/V are installed and the variable energy source v_s is again reduced such that v_c drops from 30 V to 26 V. Fig. 13(a) shows the RMS voltage of v_c being boosted up back to 30 V by activating the first ES while keeping the second ES deactivated. Fig. 13(b) shows the RMS voltage of v_c being regulated at 30 V by activating the second ES while keeping the first ES deactivated. In both the aforementioned settings, the grid voltage is stably regulated. However, when both the ES are concurrently activated, as shown in Fig. 13(c), oscillation and instability of v_c, v_{es1}, and v_{es2} occur, which validates the analysis aforementioned. Yet, based on the tuning strategy of PI controllers for ES provided and using what is given from Fig. 10, the system can be made stable by setting K_p and K_i of both ES as $K_p = 0.02$ V/V and $K_i = 0.003$ V/V. The results are given in Fig 13(d) which shows that v_c, v_{es1}, and v_{es2} can work stably and the RMS value of v_c is well regulated at 30 V. Then, three units of the smart load with the same PI controller tuning of $K_p = 0.05$ V/V and $K_i = 0.008$ V/V are installed and the variable energy source v_s is also reduced such that v_c drops from 30 V to 26 V. Fig. 14(a) shows the RMS voltage of v_c being regulated to 30 V by activating the first ES while keeping the second ES and third ES deactivated. Fig. 14(b) shows the RMS voltage of v_c regulated at 30 V by activating the second ES while keeping the first ES and third ES deactivated. Fig. 14(c) shows the RMS voltage of v_c regulated at 30 V by activating the third ES while keeping the

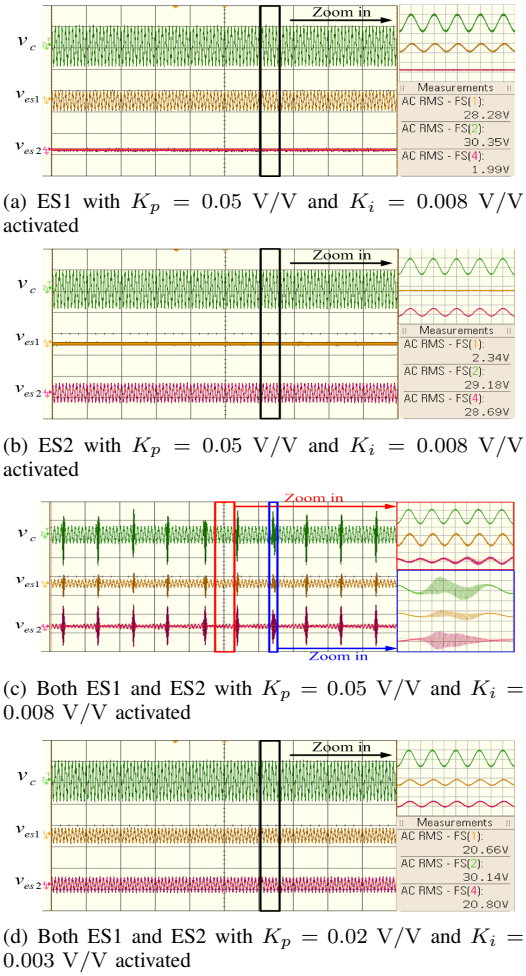

(a) ES1 with $K_p = 0.05$ V/V and $K_i = 0.008$ V/V activated

(b) ES2 with $K_p = 0.05$ V/V and $K_i = 0.008$ V/V activated

(c) Both ES1 and ES2 with $K_p = 0.05$ V/V and $K_i = 0.008$ V/V activated

(d) Both ES1 and ES2 with $K_p = 0.02$ V/V and $K_i = 0.003$ V/V activated

Fig. 13. Waveforms of the common coupling point voltage v_c, voltage of ES1, and voltage of ES2 for various settings of the ES.

first ES and second ES deactivated. In both the aforementioned settings, the grid voltage is stably regulated. However, when the three ES are concurrently activated, as shown in Fig. 14(d), oscillation and instability of v_c, v_{es1}, and v_{es2} occur, which again validates the analysis aforementioned. However, based on the tuning strategy of PI controllers for ES provided and using what is given from Fig. 10, the system can be made stable by using more stringent values of $K_p = 0.02$ V/V and $K_i = 0.003$ V/V. The results are given in Fig. 14(e), which shows that v_c, v_{es1}, v_{es2}, and v_{es3} can work stably and the RMS value of v_c is well regulated at 30 V.

Corresponding to the results and setting given in Fig. 14(d) and Fig. 14(e), the frequency of the grid due to voltage instability can be seen in Fig. 15. Apparently, without the proposed tuning method, the frequency varies out of the desired value. However, with the proposed tuning method, the frequency is kept steady at 50 Hz.

VI. Conclusions

The use of electric springs (ES) in large quantity over the power grid, even if every single ES set implemented is designed to be stable, can still suffer from stability issue if specified design are not carried out. This is due to the natural

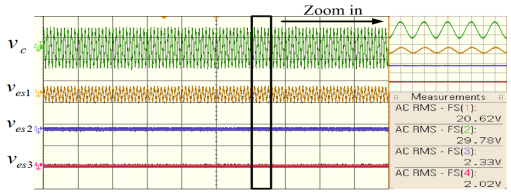

(a) ES1 with $K_p = 0.05$ V/V and $K_i = 0.008$ V/V is activated

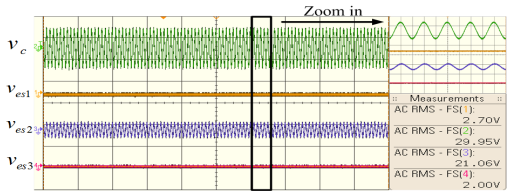

(b) ES2 with $K_p = 0.05$ V/V and $K_i = 0.008$ V/V is activated

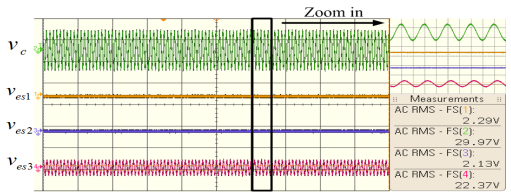

(c) ES3 with $K_p = 0.05$ V/V and $K_i = 0.008$ V/V is activated

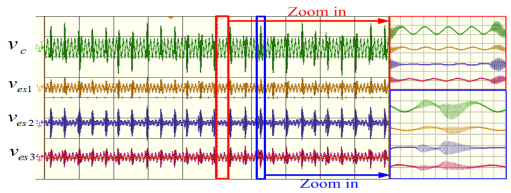

(d) ES1, ES2, and ES3 with $K_p = 0.05$ V/V and $K_i = 0.008$ V/V are activated

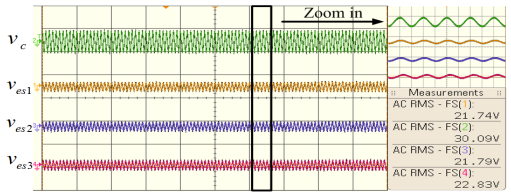

(e) ES1, ES2, and ES3 with $K_p = 0.02$ V/V and $K_i = 0.003$ V/V are activated

Fig. 14. Waveforms of the common coupling point voltage v_c, voltage of ES1, voltage of ES2, and voltage of ES3 for various settings of the ES.

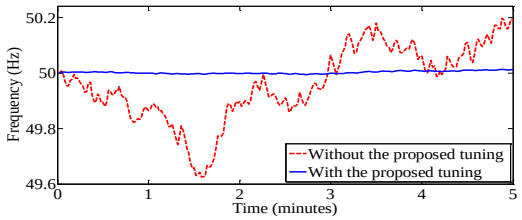

Fig. 15. Frequency of the grid when all three ES are activated with and without using the proposed tuning method.

phenomenon that multiple stable systems when combined into a new system may still be unstable. Therefore, the stability analysis and design of the ES for power grid implementation are investigated in this paper. A method for tuning K_p and K_i of the PI controllers of the ES, which will ensure overall system stability in a weak grid comprising a plurality of ES, is devised. With the validation of both simulation and experimental results, the fact that more stringent tuning of K_p and K_i of the ES is required as more ES are installed in the weak grid is uncovered. Moreover, a hypothesis that the number of ES that can be installed in the weak grid is maximized as K_p and K_i are tuned to approach the optimal values can be proposed. Besides, frequency variation of the generator, which is induced by the parallel connection of the multiple ES, can also be eliminated by the proposed tuning method.

VII. Acknowledgement

The authors would like to thank Prof. David Hill and the theme-based research project T23-701/14-N.

References

[1] "On investing in the development of low carbon technologies (SET-Plan) – A technology roadmap," Brussels, Belgium, Oct. 7, 2009.
[2] "Meeting the energy challenge – A white paper on energy," Department of Trade and Industry, U. K. Government, May 2007.
[3] "China eyes 20% renewable energy by 2020," China Daily, Jun. 10, 2009.
[4] A. Brooks, E. Lu, D. Reicher, C. Spirakis, and B. Weihl, "Demand dispatch," *IEEE Power Energy Mag.*, vol. 8, no. 3, pp. 20–29, May. 2010.
[5] S. C. Lee, S. J. Kim, and S. H. Kim, "Demand side management with air conditioner loads based on the queuing system model," *IEEE Trans. Power Syst.*, vol. 26, no. 2, pp. 661–668, Sept. 2010.
[6] M. Parvania and M. Fotuhi-Firuzabad, "Demand response scheduling by stochastic SCUC," *IEEE Trans. Smart Grid*, vol. 1, no. 1, pp. 89–98, Jun. 2010.
[7] M. Pedrasa, T. D. Spooner, and I. F. MacGill, "Scheduling of demand side resources using binary particle swarm optimization," *IEEE Trans. Power Syst.*, vol. 24, no. 3, pp. 1173–1181, Aug. 2009.
[8] A. Mohsenian-Rad, V. W. S. Wong, J. Jatskevich, R. Schober and A. Leon-Garcia, "Autonomous demand-side management based on game-theoretic energy consumption scheduling for the future smart grid," *IEEE Trans. Smart Grid*, vol. 1, no. 3, pp. 320–331, Dec. 2010.
[9] F. Kienzle, P. Ahcin, and G. Anderson, "Valuing investments in multi-energy conversion, storage, and the demand-side management systems under uncertainty" *IEEE Trans. Sustainable Energy*, vol. 2, no. 2, pp. 194–202, Apr. 2011.
[10] J. L. Woodbridge, "Application of storage betteries to regulation of alternating-current systems," *Trans. Amer. Inst. Electr. Eng.*, vol. XXVII, no. 2, pp. 987–1012, 1908.
[11] S. Y. R. Hui, C. K. Lee, and F. F. Wu, "Electric springs-A new smart grid technology," *IEEE Trans. Smart Grid*, vol. 3, no. 3, pp. 1552–1561, Sept. 2012.
[12] C. K. Lee and S. Y. R. Hui, "Reduction of energy storage requirements in future smart grid using electric springs," *IEEE Trans. Smart Grid*, vol. 4, no. 3, pp. 1282–1288, Sept. 2013.
[13] N. R. Chaudhuri, C. K. Lee, B. Chaudhuri, and S. Y. R. Hui, "Dynamic modeling of electric springs," *IEEE Trans. Smart Grid*, vol. 5, no. 5, pp. 2450–2458, Sept. 2013.
[14] C. K. Lee, N. R. Chaudhuri, B. Chaudhuri, and S. Y. R. Hui, "Droop control of distributed electric springs for stabilizing future power grid," *IEEE Trans. Smart Grid*, vol. 4, no. 3, pp. 1558–1566, Sept. 2013.
[15] X. Luo, Z. Akhtar, C. K. Lee, S. C. Tan, and S. Y. R. Hui, "Distributed voltage control with eletric springs: comparison with STATCOM," *IEEE Trans. Smart Grid*, vol. 6, no. 1, pp. 209–219, Aug. 2014.
[16] S. C. Tan, C. K. Lee, and S. Y. R. Hui, "General steady-state analysis and control principle of electric springs with active and reacitve power compensations," *IEEE Trans. Power Electron.*, vol. 28, no. 8, pp. 3958–3969, Aug. 2013.
[17] A. M. Turing, "The chemical basis of morphogenesis," *Philos. Trans. R. Soc. of Lond.*, vol. 237, no. 641, pp. 37–72, Aug. 1952.

[18] K. Mainzer and L. O. Chua, *Local Activity Principle*, London : Imperial College Press; Singapore : World Scientific, 2013.
[19] A. A. A. Radwan and Y. A. R. I. Mohamed, "Linear active stabilization of converter-dominated dc microgrids," *IEEE Trans. Smart Grid*, vol. 3, no. 1, pp. 203–216, Oct. 2011.
[20] H. Liang, B. J. Choi, W. Zhuang, and X. Shen, "Stability enhancement of decentralzed inverter control through wireless communications in microgrids," *IEEE Trans. Smart Grid*, vol. 4, no. 1, pp. 321–331, Feb. 2013.
[21] M. Ashabani and Y. A. R. I. Mohamed, "Novel comprehensive control framework for incorporating VSCs to power grids using bidirectional synchronous-VSC," *IEEE Trans. Power Syst.*, vol. 29, no. 2, pp. 943–957, Nov. 2013.
[22] J. Huang, K. A. Corzine, and M. Belkhayat, "Small-signal impedance measurement of power-eletronics-based ac power systems using line-to-line current injection," *IEEE Trans. Power Electron.*, vol. 24, no. 2, pp. 445–455, Feb. 2009.
[23] X. Lu, K. Sun, L. Huang, M. Liserre, and F. Blaabjerg, "An active damping method based on biquad digital filter for parallel grid-interfacing inverters with LCL," in *Proc. of Applied Power Electronics Conference and Exposition (APEC)*, 2014, pp. 392–397.
[24] N. Pogaku, M. Prodanović, and T. C. Green, "Modeling, analysis and testing of autonomous operation of an inverter-based microgrid," *IEEE Trans. Power Electron.*, vol. 22, no. 2, pp. 613–625, Mar. 2007.
[25] S. V. Iyer, M. N. Belur, and M. C. Chandorkar, "A generalized computational method to determine stability of a multi-inverter microgrid," *IEEE Trans. Power Electron.*, vol. 25, no. 9, pp. 2420–2432, Apr. 2010.
[26] Y. A. I. Mohamed and E. F. El-Saadany, "Adaptive decentralized droop controller to preserve power sharing stability of paralleled inverters in distributed generation microgrids," *IEEE Trans. Power Electron.*, vol. 23, no. 6, pp. 2806–2816, Dec. 2008.
[27] Z. Yao, L. Xiao, and Y. Yan, "Control strategy for series and parallel output dual-buck half bridge inverters based on DSP control," *IEEE Trans. Power Electron.*, vol. 24, no. 2, pp. 434–444, Dec. 2008.
[28] N. Bottrell, M. Prodanovic, and T. C. Green, "Dynamic stability of a microgrid with an active load," *IEEE Trans. Power Electron.*, vol. 28, no. 11, pp. 5107–5119, Jan. 2013.
[29] M. Borrega, L. Marroyo, R. Gonzalez, J. Balda, and J. L. Agorreta, "Modeling and control of a masterslave PV inverter with n-paralleled inverters and three-phase three-limb inductors," *IEEE Trans. Power Electron.*, vol. 28, no. 6, pp. 2842–2855, Sept. 2012.
[30] D. Jovcic, N. C. Pahalawaththa, and M. Zavahir, "Inverter controller for HVDC systems connected to weak AC systems," *IEE Proc. Gener. Transm. Distrib.*, vol. 146, no. 3, pp. 235–240, May 1999.
[31] U. S. -Canada Power System Outage Task Force, "Final report on the August 14, 2003 blackout in the United States and Canada: causes and recommendations," Apr. 2004.
[32] Power Systems Enguineering Research Center, "Selected information about the July 31 blackout in India affecting the northern and eastern regions," Aug. 2012.
[33] D. M. Mitchell, *DC-DC Switching Regulator Analysis*, New York: McGraw-Hill, 1988.
[34] H. Bindner, "Power control for wind turbines in weak grids: concepts development," Riso National Lab., Roskilde, Riso-R-1118 (EN), Mar. 1999.
[35] K. Ogata, *Modern Control Engineering*, NJ : Prentice Hall, 2010.
[36] N. H. Abel, "Démonstration de l'impossibilité de la résolution algébrique des équations générales qui passent le quatrième degré," *Journal de Crelle*, t. 1, 1826
[37] P. M. Anderson and A. A. Fouad, *Power System Control and Stability*, Ames, IA : Iowa State Univ. Press, 1977.

Yun Yang (S'13) received the B.S. degree from Wuhan University, Wuhan, China, in 2012. He is currently working toward the Ph.D. degree in Power Electronics Research Group, Department of Electrical and Electronic Engineering, The University of Hong Kong, Hong Kong. His current research interests include variable structure control and predictive control of power electronics for smart grids and LED lightings.

Siu-Shing Ho received the BEng degree in electronic engineering at City University of Hong Kong in 2008. From 1996 to 2006, he was an electronic engineer in the Astec Custom Power (HK) LTD. He is a Research Associate in Power Electronics Research Group, University of Hong Kong. His research interests include control of power electronics and smart grid.

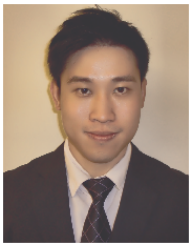

Siew-Chong Tan (M'06–SM'11) received the B.Eng. (Hons.) and M.Eng. degrees in electrical and computer engineering from the National University of Singapore, Singapore, in 2000 and 2002, respectively, and the Ph.D. degree in electronic and information engineering from the Hong Kong Polytechnic University, Hong Kong, in 2005.

From October 2005 to May 2012, he worked as Research Associate, Postdoctoral Fellow, Lecturer, and Assistant Professor in Department of Electronic and Information Engineering, Hong Kong Polytechnic University, Hong Kong. From January to October 2011, he was Senior Scientist in Agency for Science, Technology and Research (A*Star), Singapore. He is currently an Associate Professor in Department of Electrical and Electronic Engineering, The University of Hong Kong, Hong Kong. Dr. Tan was a Visiting Scholar at Grainger Center for Electric Machinery and Electromechanics, University of Illinois at Urbana-Champaign, Champaign, from September to October 2009, and an Invited Academic Visitor of Huazhong University of Science and Technology, Wuhan, China, in December 2011. His research interests are focused in the areas of power electronics and control, LED lightings, smart grids, and clean energy technologies.

Dr. Tan serves extensively as a reviewer for various IEEE/IET transactions and journals on power, electronics, circuits, and control engineering. He is an Associate Editor of the IEEE Transactions on Power Electronics. He is a coauthor of the book *Sliding Mode Control of Switching Power Converters: Techniques and Implementation* (Boca Raton: CRC, 2011).

S. Y. (Ron) Hui (M'87–SM'94–F'03) received his BSc (Eng) Hons at the University of Birmingham in 1984 and a D.I.C. and PhD at Imperial College London in 1987. Currently, he is the holder of the Philip Wong Wilson Wong Chair Professorship at the University of Hong Kong. Since July 2010, he has concurrently held a part-time Chair Professorship of Power Electronics at Imperial College London.

He has published over 300 technical papers, including more than 200 refereed journal publications and book chapters. Over 55 of his patents have been adopted by industry. He is an Associate Editor of the IEEE Transactions on Power Electronics and IEEE Transactions on Industrial Electronics. In 2010, he received the IEEE Rudolf Chope R&D Award from the IEEE Industrial Electronics Society, the IET Achievement Medal (The Crompton Medal) and was elected to the Fellowship of the Australian Academy of Technological Sciences & Engineering. He is the recipient of the 2015 IEEE William E. Newell Power Electronics Award.